# Investigation of the Dimerization of Proteins from the Epidermal Growth Factor Receptor Family by Single Wavelength Fluorescence Cross-Correlation Spectroscopy

Ping Liu,*† Thankiah Sudhaharan,†‡ Rosita M. L. Koh,† Ling C. Hwang,* Sohail Ahmed,‡ Ichiro N. Maruyama,†§ and Thorsten Wohland*

*Department of Chemistry, National University of Singapore, Singapore; †Proteomics Group, Genome Institute of Singapore, Singapore; ‡Centre for Molecular Medicine, Singapore; and §Molecular Neuroscience Unit, Okinawa Institute of Science and Technology, Okinawa, Japan

ABSTRACT Single wavelength fluorescence cross-correlation spectroscopy (SW-FCCS), introduced to study biomolecular interactions, has recently been reported to monitor enzyme activity by using a newly developed fluorescent protein variant together with cyan fluorescent protein. Here, for the first time to our knowledge, SW-FCCS is applied to detect interactions between membrane receptors in vivo by using the widely used enhanced green fluorescent protein and monomeric red fluorescent protein. The biological system studied here is the epidermal growth factor/ErbB receptor family, which plays pivotal roles in the development of organisms ranging from worms to humans. It is widely thought that a ligand binds to the monomeric form of the receptor and induces its dimeric form for activation. By using SW-FCCS and Förster resonance energy transfer, we show that the epidermal growth factor receptor and ErbB2 have preformed homo- and heterodimeric structures on the cell surface and quantitation of dimer fractions is performed by SW-FCCS. These receptors are major targets of anti-cancer drug development, and the receptors' homo- and heterodimeric structures are relevant for such developments.

## INTRODUCTION

Fluorescence cross-correlation spectroscopy (FCCS) is a versatile technique for the quantitation of protein-protein interactions in live cells (1). It is derived from fluorescence correlation spectroscopy (2) and is a technique to measure molecular interactions with single molecule sensitivity, independent of the size and mass of molecules under investigation. Its first application to molecular interactions was shown by Schwille et al. (3), and theories for ligand-receptor interactions have previously been described (4,5). However, the first FCCS experiments used either two distinct lasers for excitation (3) or two-photon excitation by a pulsed laser (6). Application of FCCS to in vivo measurements has been reviewed recently (7) and the use of fluorescent proteins (FPs) for FCCS has been demonstrated (5,8,9). However, the use of two lasers or of one pulsed laser makes the setup either difficult to align or expensive (6,10,11). SW-FCCS has been shown to work using a combination of fluorescent and scattered light (12) and has recently been applied to the analysis of biomolecular interactions using only fluorescence labels (13–15). For the first time we performed single wavelength fluorescence cross-correlation spectroscopy (SW-FCCS) on FP-fusion receptors on the surface of single live cells to quantitatively measure the receptor dimer fraction, using the most widely used green fluorescent protein (GFP) and monomeric red fluorescent protein (mRFP) (16). Due to the long tail of the excitation spectrum it is possible to excite both fluorophores with similar efficiencies at a wavelength of 514 nm. In addition to the use of recently developed FP mutants with a large Stokes shift (8), this method offers the advantage of more stable fluorophores and a longer excitation wavelength, limiting cell damage and autofluorescence.

Förster resonance energy transfer (FRET) is also often considered an excellent method to monitor the interaction of proteins within a microenvironment of 10 nm distance in single cells in the native form (17), and has the potential to address a large number of highly significant structural information within the cell without loosing the information on small changes (18). It is based on the nonradiative energy transfer between a donor and acceptor fluorophore pair in which the emission spectrum of the donor overlaps with the excitation spectrum of the acceptor (19,20).

Epidermal growth factor receptor (EGFR) signaling is involved in diverse physiological processes such as cell proliferation and apoptosis. Upregulation of the EGFR/ErbB family tyrosine kinase activity is frequently implicated in a variety of human cancers (21). Ligand-induced dimerization is proposed as a molecular mechanism underlying the activation of all the growth factor receptor tyrosine kinases including EGFR and ErbB2, also called HER2 or Neu (22,23). Before ligand binding, however, it remains controversial whether the receptor has a monomeric or dimeric structure (24–28). Chemical cross-linking and coimmunoprecipitation

*Submitted November 27, 2006, and accepted for publication March 26, 2007.*

Ping Liu and Thankiah Sudhaharan contributed equally to this work.

Address reprint requests to Thorsten Wohland, E-mail: chmwt@nus.edu.sg; or Ichiro N. Maruyama, E-mail: ichi@oist.jp.

Rosita M. L. Koh's present address is Institute of Molecular and Cell Biology, 61 Biopolis Dr., Singapore 138673, Singapore.

Ling C. Hwang's present address is Dept. of Physics, Clarendon Laboratory, University of Oxford, Parks Rd., Oxford OX13PU, UK.

Editor: Thomas Schmidt.



0006-3495/07/07/684/15 $2.00

doi: 10.1529/biophysj.106.102087

have most commonly been used to detect dimers of the cell-surface receptors. Unfortunately, all the chemical cross-linkers are too unstable in aqueous buffer to quantitatively trap the dimer (24,29), particularly at physiological expression levels ($<10^5$ molecules per cell (30)). Meanwhile, coimmunoprecipitation cannot directly address whether the receptor has a dimeric structure, although it can detect the receptor's complex in which they may not directly interact with each other as a dimer. Because the dimeric structure might also be unstable against detergent solubilization (24), the structural analysis should be conducted in vivo on the surface of live cells. In this study, therefore, we tried to detect cross correlation and FRET due to homo- and heterodimeric structures to examine the receptor's ternary structure on the live cell surface.

Thus by the novel combination of two methods, SW-FCCS and FRET, we could demonstrate the preformed EGF/ErbB2 receptors homo- and heterodimers in the native form in single live cells. Most of the studies on the ErbB family receptors by fluorescence techniques that have been reported were done through either ligand labeling or antibody conjugation, and measurements were carried out on cell lines overexpressing the receptors (27,31,32). Here we mainly focused on cells that express physiological levels of the receptors in the absence of ligand stimulation. Although Clayton et al. reported the preformed homodimeric structure of EGFR before activation (30), we further investigated the heterodimeric structure between EGFR and ErbB2.

## MATERIALS AND METHODS

### Construction of plasmids encoding chimeras between EGFR or ErbB2 and FPs

pNUT/EGFR plasmid DNA (24) was digested with *Kpn*I, and the resulting fragment ends were repaired by treatment with T4 DNA polymerase. A 3.5-kb *Kpn*I-*Bgl*II fragment encoding the N-terminal peptide of EGFR was excised out from the fragment by digesting with *Bgl*II. A 0.8-kb fragment encoding the C-terminus of EGFR was amplified by polymerase chain reaction (PCR) with the following oligonucleotide primers encoding *Bgl*II and *Age*I sites (underlined), respectively: 5′-CCAGCGAGATCTCCTCCATCC and 5′-CCTCCGTA*CCGGT*GCTCCAATAAATTCACTGC. The latter primer also encodes a proline residue at the stop codon indicated in italic. The resulting PCR fragment was digested with *Bgl*II and *Age*I, and cloned with the 3.5-kb *Kpn*I-*Bgl*II fragment in tandem into pEGFP-N1, pECFP-N1, and pEYFP-N1 (Clontech, Palo Alto, CA) digested with *Afe*I and *Age*I to make plasmid constructs encoding EGFR-GFP, EGFR-CFP, and EGFR-YFP chimeras, respectively. A plasmid encoding an EGFR-mRFP fusion protein was constructed by replacing the GFP gene of EGFR-GFP with a PCR product amplified from pRSETB/mRFP, kindly provided by Roger Tsien, University of California at San Diego, using the following primers with an *Age*I or *Not*I site (underlined), respectively: 5′-GATCCACCGGTCGCCACCATGGCCTCCTCCGAGGACGTC, or 5′-TTTTCCTTTTGCGGCCGCTTAGGCGCCGGTGGAGTG.

As negative controls, we also made plasmids encoding FPs fused to the plasma membrane target (PMT) sequence at the FP's N-terminus. The YFP gene was amplified from pEYFP-N1 by PCR using a pair of primers, 5′-*AGCAAGCGGCGGAAGGCCGACAAGGAGAGC*ATGGTGAGCAAGGGC (PMS1) and 5′-TTTTCCTTTTGCGGCCGCTTACTTGTACAGCTCGTCC (PMS5). PMS1 encodes part of the PMT sequence (in italic) of the X-linked retinitis pigmentosa protein RP2 (33), and PMS5 encodes a *Not*I site (underlined). The resulting PCR product was then used as a template for the second round of PCR with primers, 5′-GATCCACCGGT*ATGGGCTGCTTCTTCAGCAAGCGGCGGAAG* (PMS2), which encodes an *Age*I site (underlined) and the remaining sequence of PMT (in italic), and PMS5. To construct a plasmid encoding a chimera, PMT-YFP, the resulting PCR product was then doubly digested with *Age*I and *Not*I, and was cloned into pECFP-N1 from which the FP gene was removed by digesting with *Age*I and *Not*I. Similarly, plasmids encoding PMT-CFP, PMT-GFP, and PMT-mRFP were also made. Another negative control we used for SW-FCCS is the cytosolic GFP/mRFP pair, in which the mRFP construct was simply amplified from pRSETB/mRFP vector and inserted into pEGFP-N1 vector (Clontech) by replacing the EGFP sequence through *Age*I and *Not*I sites.

A plasmid encoding a positive control, PMT-CFP-YFP, for the FRET experiment was constructed in the following manner: the CFP gene was amplified from pECFP-N1 using PMS1 and PMS3 (5′-GCTCACCATGCCGCTCCCGGACCCCTTGTACAGCTCGTC) as primers, and the resulting PCR product was then used for the second round of PCR using PMS2 and PMS3 as primers. The YFP gene was also amplified by using a pair of primers, 5-GGGTCCGGGAGCGGCATGGTGAGCAAGGGC (PMS4) and 5′-GATCTAGAGGTCGCGGCCGCT (PMC1). The PMS4 encodes a five-amino acid residue linker (underlined), and PMC1 encodes *Not*I (underlined). These amplified CFP and YFP gene products were then used for overlap extension PCR (34) using primers, PMS2 and PMC1, to yield a full-length PMT-CFP-YFP chimera. The resulting PCR product was digested with *Age*I and *Not*I, and then cloned into pEGFP-N1 from which the GFP gene was removed by digestion with the two enzymes.

To construct plasmids encoding ErbB2-GFP, ErbB2-CFP, and ErbB2-YFP, a 0.8-kb 3′-terminal fragment of the ErbB2 gene was amplified from pcDNA/ErbB2 (provided by Haihe Wang, Institute of Molecular and Cell Biology, Singapore), in which the full-length human ErbB2 cDNA was cloned between *Nhe*I and *Not*I sites of pcDNA 3.1/Zeo plasmid vector (Invitrogen, Carlsbad, CA), by PCR using a pair of primers, 5′-CTCCCGCATGGCCAGGGAC (primer A; this sequence resides upstream of a unique *Afe*I site of the ErbB2 cDNA) and 5′-CACCATCCCTCCACTCCCACTCCCTCCCACTGGCACGTCCAGACCCAGGTAC (primer B). The primer B encodes a seven amino-acid residue linker that replaces the stop codon. The GFP gene was also similarly amplified from pEGFP-N1 using a pair of primers, 5′-GCCAGTGGGAGGGAGTGGGAGTGGAGGGATGGTGAGCAAGGGCGAGGAGCTG (primer C) and 5′-GTCGCGGCCGCTTTACTTGTACAGCTCGTCC (primer D), which encodes *Not*I (underlined). On the primers B and C, a seven amino-acid residue linker was also underlined. The two PCR products were mixed for overlap extension PCR with primers A and D, and the resulting product was digested with *Afe*I and *Not*I. The fragment was cloned into pcDNA/ErbB2 digested with the two enzymes, resulting in pcDNA/ErbB2-GFP. A plasmid encoding ErbB2-mRFP was similarly constructed from a PCR product amplified from pRSETB/mRFP using primers, 5′-GCCAGTGGGAGGGAGTGGGAGTGGAGGGATGGCCTCCTCCGAGGACGTCATC and 5′-GTCGCGGCCGCTTAGGCGCCGGTGGAGTGGCG.

To make the amino-terminal fusion construct of EGFR with FP, an *Xho*I restriction site was created just after the signal peptide cleavage site of EGFR by site-directed mutagenesis using a QuickChange XL kit (Stratagene, La Jolla, CA), pNUT/EGFR as a template, and the following mutagenic primers: 5′-CCGGCGAGTCGGGCTCTCGAGGAAAAGAAAGTTTGC and 5′-TTGGCAAACTTTCTTTTCCTCGAGAGCCCGACT, in which mutation sites are underlined. To construct an expression plasmid encoding mRFP-EGFR, the mRFP gene was amplified by PCR from pRSETB/mRFP with the following primers: 5′-GCGCGCCTCGAGATGGCCTCCTCCGAGGACGTC and 5′-GCGCGCCTCGAGACTCCCACTCCCTCCGGATCCGGCGCCGGTGGAGTGGCG, in which *Xho*I sites are indicated by underlines. The resulting PCR product was digested with *Xho*I and cloned into the *Xho*I site of the EGFR gene of pNUT/EGFR(*Xho*I) to make pNUT/

mRFP-EGFR(*Xho*I) encoding mRFP-EGFR, in which mRFP was fused to the amino-terminus of EGFR. To create a plasmid encoding mRFP-EGFR-GFP, the pNUT/mRFP-EGFR plasmid was digested with *Sma*I and *Age*I, and a 6.8-kb fragment lacking the carboxyl-terminus of EGFR was purified after blunting the *Age*I end with T4 DNA polymerase. A 3.6-kb *Sma*I-*Not*I fragment of pEGFP-N1/EGFR-GFP was also purified after blunting the *Not*I end, and cloned into the 6.8-kb fragment of pNUT/mRFP-EGFR to make pNUT/mRFP-EGFR-GFP. In the similar way, plasmids encoding CFP-EGFR-YFP or YFP-EGFR-CFP were also constructed from CFP and YFP fragments amplified using a pair of primers; 5′-GCGCGCCTCGAGATGG-TGAGCAAGGGC and 5′-GCGCGCCTCGAGACTCCCACTCCCTCCG-GATCCCTTGTACAGCTCGTC.

All the constructs described above were confirmed by DNA sequencing. A schematic drawing of the constructs is shown in Fig. 1 *A*.

## Cell culture and expression of receptor chimera with FP

As introduced above, EGFR and ErbB2 cDNAs were modified so that the clones can produce the receptor proteins fused with FPs at its carboxyl/amino-terminus through a linker sequence. CHO-K1 cells purchased from ATCC (Manassas, VA) were cultivated in Ham's F12 medium (with Kaighn's modification) supplemented with 2 mM L-glutamine, 1.5 g/L sodium bicarbonate, 50 U/ml penicillin G, 50 $\mu$g/ml streptomycin, and 10% fetal bovine serum (FBS) at 37°C in 5% (v/v) $CO_2$ humidified atmosphere. For the coexpression of two different fusion constructs, the ratio of the amounts of the two plasmids was kept at 1:1 (2 $\mu$g EGFR-GFP/2 $\mu$g EGFR-mRFP, for example) for transfection. For the triple expression of FP-fusion plasmids and one wild-type (wt) receptor plasmid (pNUT/EGFR), the ratio among the three plasmids was 1:1:0.5 and 1:1:1, respectively. Two methods were mainly used to introduce plasmids DNA into CHO cells, electroporation (Bio-Rad, Hercules, CA) and Fugene 6 transfection kit (Roche Diagnostics, Singapore), and no difference in dimerization of the receptors was observed between the two transfection methods. For electroporation, ~90% confluent cells in a flask were washed once with 1× phosphate buffered saline (PBS), trypsinized with 0.25% trypsin-0.03% EDTA solution for 5 min at 37°C, and then resuspended in culture medium. Cells (~1 × $10^6$) were precipitated by centrifugation and resuspended in culture medium in an electroporation cuvette, 2-mm wide. After mixing the cells with DNA, 10 $\mu$g in total, the cuvette was chilled on ice for 10 min. GenePulser Xcell (Bio-Rad) was used for electroporation by following the manufacturer's preprogrammed protocol for CHO cells. After electroporation, cells were left for 10 min at room temperature, and ~50,000 cells/well were seeded in wells of a six-well plate containing

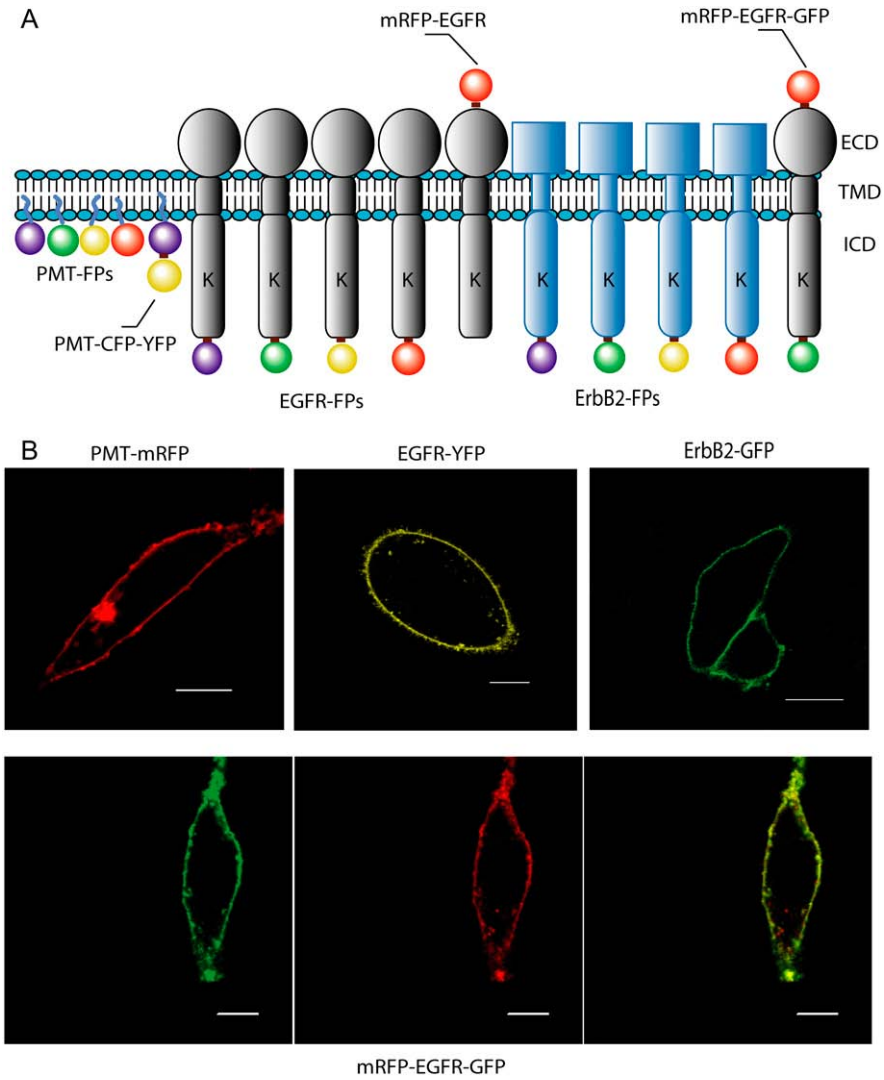


FIGURE 1 (*A*) Schematic overview of FP-fusion constructs. PMT-FPs, (from *left to right*) PMT-CFP, PMT-GFP, PMT-YFP, and PMT-mRFP. EGFR-FPs and ErbB2-FPs are listed in the same order. ECD, extracellular domain; TMD, transmembrane domain; ICD, intracellular domain; K, kinase domain. (*B*) Example images of cells expressing different constructs. mRFP-EGFR-GFP, positive control for SW-FCCS. (*Left*) Image in GFP channel, (*middle*) image in mRFP channel, and (*right*) overlapping image. Note that mRFP and GFP images do not completely overlap each other possibly due to the cleavage of FP through the receptor's recycling. Bar, 10 $\mu$m.

prewashed coverglasses (30 mm in diameter; Lakeside, Monee, IL). For Fugene 6 transfection, cells were seeded in six-well plates containing the 30-mm coverglasses at $1 \times 10^5$ cells/well one day before transfection. CHO cells were transfected with plasmids by following the standard Fugene 6 protocol (Roche). Two days after transfection, cells were washed once with 1× PBS, and were further cultivated in F12K medium containing 0.1% FBS, 50 U/ml penicillin G, and 50 $\mu$g/ml streptomycin for 8–16 h.

At the time of observation, cells were treated under different conditions according to different experimental targets. To observe effective internalization of the fusion receptors, cells were washed several times with 1× PBS and covered with D-MEM/F-12K medium lacking of phenol red in a POC minichamber (Carl Zeiss, Jena, Germany), and confocal imaging of the fusion receptor internalization was done at 37° by using a heating stage and a temperature regulator ''Tempcontrol 37-2 digital'' (Carl Zeiss). To keep a low fluorescence background during FRET measurements, cells were washed once with 1× PBS and covered with Hanks' balanced salt solution lacking phenol red in the minichamber for FRET measurements. For FCCS measurements, cells were washed thoroughly with 1× PBS and covered with 1 ml 1× PBS in the minichamber during measurements. EGF was added in two experiments, confocal imaging of the fusion receptor internalization and SW-FCCS observation on the fusion receptors after EGF stimulation. The final concentration of EGF was kept at 100 ng/ml for both internalization imaging and SW-FCCS observation. Because SW-FCCS mainly focused on cell membrane, to avoid fast internalization of the membrane receptors after EGF activation during SW-FCCS observation, cells were incubated with endocytosis inhibitors one-half hour before adding EGF. The final concentration of the inhibitors was $NaN_3$ (Sigma, St. Louis, MO), 10 mM; NaF (Sigma), 2 mM; 2-deoxy-D-glucose (Sigma), 5 mM, respectively.

Fig. 1 *B* shows some example images of cells expressing FP-fusion constructs. Fluorescence was clearly shown on cell membrane, which suggests that FP-fusion does not affect the translocation of the receptors. Cell images were taken on a Zeiss laser scanning confocal microscope LSM510 META (Carl Zeiss). The imaging of FP-fusion EGFR internalization after ligand stimulation was also carried out on a laser scanning confocal microscope LSM510 (Carl Zeiss).

## Phosphorylation assay of receptor chimera with FP

To analyze autophosphorylation activity of the chimeric EGFR constructs, the expression plasmid vector DNAs, 2–8 $\mu$g each, were introduced into COS-7 cells (ATCC), $\sim 1 \times 10^6$ cells per tube, by using a Nucleofector II (amaxa GmbH, Germany) under preset conditions by the manufacturer. After cultivating the transfected cells for two days in a culture dish (6 cm in diameter), cells ($\sim 3 \times 10^6$) were starved in the absence of serum for 24 h, and were then stimulated with 100 ng/ml (a final concentration) of EGF on ice for 30 min (24). After washing three times with ice-cold 1× PBS, the cells were solubilized with 1× Laemmli sample buffer (100 $\mu$l; Bio-Rad) supplemented with 1.0 mM $Na_3VO_4$ and 5% mercaptoethanol, and were heat denatured for 10 min at 95°C. Samples were stored at −86°C until use. An aliquot, 2–40 $\mu$l each per lane, of the samples was electrophoretically separated with a 7% SDS-polyacrylamide gel, and blotted onto a Hybond-P PVDF membrane (pore size, 0.45 $\mu$m; GE Healthcare, Little Chalfont, UK). After blocking the membrane with 5% skimmed milk in TBS buffer (20 mM Tris-Cl, pH 7.4, 150 mM NaCl, 0.1% Tween-20), EGFR chimera and its phosphorylated form were stained with anti-EGFR antibody (Ab-12; Lab Vision, Fremont, CA), and followed by incubating with a secondary antibody, sheep anti-mouse IgG conjugated with horseradish peroxidase. For the detection of a phosphorylated form of the receptors, alternatively, the membrane was blocked with a mixture of Blocking One-P (Nakalai Tesque, Kyoto, Japan), 2% ECL Blocking reagent (GE Healthcare), and 50 mM NaF, and was subjected for binding with anti-pTyr (PY20) antibody (sc-508; Santa Cruz Biotech., Santa Cruz, CA) as a primary antibody and then with a secondary antibody as described above. The proteins were visualized by treating the membrane with an ECL Western blotting detection kit (GE Healthcare), and were analyzed by using a Fujifilm Luminescent Image Analyzer (LAS-3000; Tokyo, Japan).

## SW-FCCS setup

SW-FCCS was carried out on a modified Zeiss Axiovert 200 inverted microscope as described elsewhere (13). For SW-FCCS measurements of FP-fused EGFR and ErbB2, an excitation wavelength of 514 nm (argon ion laser; Spectra-Physics, Mountain View, CA) at 40–70 $\mu$W was used. The excitation light was reflected by a dichroic mirror, 525DRLP (Omega Optical, Brattleboro, VT), and focused by a water-immersion objective (63×, NA 1.2; Carl Zeiss) into samples. Fluorescence light was spatially filtered through a 50-$\mu$m pinhole (Linos, Heidelberg, Germany) and was split by a second dichroic mirror, 560DCLP (Omega), into two detection channels, green and red. Two band-pass filters, 545AF35 and 615DF45 (Omega), were placed in front of the avalanche photodiode detectors (SPCM-AQR-14, Pacer Components, Berkshire, UK), to further restrict the emission wavelengths for the green and red channels, respectively. Measurements were taken over 30 s for all experiments. Autocorrelations and cross correlations were simultaneously calculated by using a hardware correlator (Flex-02-12D; correlator.com, Zhejiang, China), and fitting of the correlation functions was carried out with Igor Pro 4.0 (Wavemetrics, Portland, OR). As mentioned before, SW-FCCS measurements on transfected cells were done in a POC minichamber containing 1× PBS (1 ml) after washing the cells thoroughly with 1× PBS. All the measurements were done at room temperature. Data are presented as the mean ± SD, or mean ± SE, and differences between groups were compared using Student's *t*-test (one-tailed).

## SW-FCCS calculation on the fractions of dimers

In fluorescence correlation methods the count rate per particle and second (cps) is an important factor determining the amplitude of the correlation function. Thus these values have to be known for each fluorophore and channel. We have adopted the following naming convention:

$\eta_g^G$, cps of EGFR-GFP in the green channel.
$\eta_r^G$, cps of EGFR-GFP in the red channel.
$\eta_g^R$, cps of EGFR-mRFP, or mRFP-EGFR in the green channel.
$\eta_r^R$, cps of EGFR-mRFP, or mRFP-EGFR in the red channel.
$\beta_g$, background count rate in the green channel on a cell membrane.
$\beta_r$, background count rate in the red channel on a cell membrane.

For the calculation of dimer percentages we assume that the count rate of doubly labeled molecules is just the sum of the count rates of the singly labeled molecules because in general there was no FRET observed between GFP and mRFP in our system:

$$\eta_g^{2G} = 2\eta_g^G, \tag{1}$$

$$\eta_r^{2G} = 2\eta_r^G, \tag{2}$$

$$\eta_g^{2R} = 2\eta_g^R, \tag{3}$$

$$\eta_r^{2R} = 2\eta_r^R, \tag{4}$$

$$\eta_g^{GR} = \eta_g^G + \eta_g^R, \tag{5}$$

and

$$\eta_r^{GR} = \eta_r^G + \eta_r^R. \tag{6}$$

Cross- and autocorrelation functions for this case are given by:

$$G_x(0) = \frac{\eta_g^G \eta_r^G c^G + \eta_g^R \eta_r^R c^R + \eta_g^{2G} \eta_r^{2G} c^{2G} + \eta_g^{2R} \eta_r^{2R} c^{2R} + \eta_g^{GR} \eta_r^{GR} c^{GR}}{N_A V_{eff}\left(\eta_g^G c^G + \eta_g^R c^R + \eta_g^{2G} c^{2G} + \eta_g^{2R} c^{2R} + \eta_g^{GR} c^{GR} + \beta_g/(N_A V_{eff})\right)} \times \left(\eta_r^G c^G + \eta_r^R c^R + \eta_r^{2G} c^{2G} + \eta_r^{2R} c^{2R} + \eta_r^{GR} c^{GR} + \beta_r/(N_A V_{eff})\right)^{-1}, \quad (7)$$

$$G_g(0) = \frac{\left(\eta_g^G\right)^2 c^G + \left(\eta_g^R\right)^2 c^R + \left(\eta_g^{2G}\right)^2 c^{2G} + \left(\eta_g^{2R}\right)^2 c^{2R} + \left(\eta_g^{GR}\right)^2 c^{GR}}{N_A V_{eff}\left(\eta_g^G c^G + \eta_g^R c^R + \eta_g^{2G} c^{2G} + \eta_g^{2R} c^{2R} + \eta_g^{GR} c^{GR} + \beta_g/(N_A V_{eff})\right)^2}, \quad (8)$$

and

$$G_r(0) = \frac{\left(\eta_r^G\right)^2 c^G + \left(\eta_r^R\right)^2 c^R + \left(\eta_r^{2G}\right)^2 c^{2G} + \left(\eta_r^{2R}\right)^2 c^{2R} + \left(\eta_r^{GR}\right)^2 c^{GR}}{N_A V_{eff}\left(\eta_r^G c^G + \eta_r^R c^R + \eta_r^{2G} c^{2G} + \eta_r^{2R} c^{2R} + \eta_r^{GR} c^{GR} + \beta_r/(N_A V_{eff})\right)^2}, \quad (9)$$

where concentrations are denoted by a $c$ (13,14). The superscript G and R refer to EGFR-GFP and EGFR-mRFP monomers, respectively. The superscript 2G or 2R refers to EGFR-GFP/-GFP or EGFR-mRFP/-mRFP dimers, whereas GR refers to mixed dimers of EGFR-GFP/-mRFP. $N_A$ is Avogadro's number and $V_{eff}$ is the effective observation volume. It should be noted that the actual values of $N_A V_{eff}$ has no influence on our results since only relative molecular fractions are determined but no absolute concentrations.

We assume that dimerization does not depend on FPs attached to the receptor, and this is supported by the fact that amino- and carboxyl-fusion constructs show similar dimerization (see Table 1). Therefore, the formation of dimers containing GFP/GFP, mRFP/mRFP, mRFP/GFP, and GFP/mRFP is equally likely and their occurrence depends only on the absolute amounts of GFP- and mRFP-labeled molecules present. For instance, the formation of an EGFR-GFP/-mRFP dimer depends on the probability of finding an EGFR dimer, $p_D$, times the probability of finding an EGFR-GFP, $p_G$, times the probability of finding an EGFR-mRFP, $p_R$. The probability $p_D$ of dimer formation depends on the affinity of the EGFR for itself. The probability $p_G$ is determined by the total number of EGFR-GFP divided by the total concentration of EGFR molecules. Similarly the probability $p_R$ is determined by the total number of EGFR-mRFP divided by the total concentration of EGFR molecules, $c_{tot}$:

$$c_{tot} = c^G + c^R + 2(c^{2R} + c^{2G} + c^{GR}) \quad (10)$$

$$p_G = \frac{c^G + 2c^{2G} + c^{GR}}{c_{tot}} \quad (11)$$

$$p_R = \frac{c^R + 2c^{2R} + c^{GR}}{c_{tot}} \quad (12)$$

$$c^{2G} = p_D p_G^2 c_{tot} \quad (13)$$

$$c^{2R} = p_D p_R^2 c_{tot} \quad (14)$$

$$c^{GR} = 2 p_D p_G p_R c_{tot} \quad (15)$$

$$\frac{c^{2G}}{c^{GR}} = \frac{p_G}{2 p_R} = \frac{c^G + 2c^{2G} + c^{GR}}{2(c^R + 2c^{2R} + c^{GR})}, \quad (16)$$

and

$$\frac{c^{2R}}{c^{GR}} = \frac{p_R}{2 p_G} = \frac{c^R + 2c^{2R} + c^{GR}}{2(c^G + 2c^{2G} + c^{GR})}. \quad (17)$$

Equations 7–9, 16, and 17 are solved numerically for $c^G$, $c^R$, $c^{2G}$, $c^{2R}$, and $c^{GR}$. The percentage of dimerization is then calculated by

$$f = \frac{2(c^{2G} + c^{2R} + c^{GR})}{c_{tot}}. \quad (18)$$

To extract values for Eqs. 7–9, all experimental data have been fitted to a two-dimensional model for membrane diffusion:

$$G(\tau) = \frac{1}{N}\left(1 + \frac{4D\tau}{\omega^2}\right)^{-1}\left(\frac{Te^{-\tau/\tau_T}}{1-T} + 1\right) + G_\infty. \quad (19)$$

$N$ is the average number of particles in the confocal volume. $D$ is the diffusion coefficient of the receptors in the membrane, and $\omega$ is the radial distances of the confocal volume at which the intensity has dropped by $1/e^2$

**TABLE 1 Homo- and heterodimer fractions of EGFR and ErbB2 (including third unlabeled receptor competition) on the cell surface**

| Construct | Dimer % (± SD) | Dimer % (± SE) | Normalized dimer % (± SE) | Sample size ($n$) |
|---|---|---|---|---|
| Cytosolic GFP/mRFP (negative) | 17 ± 9 | 17 ± 2 | 23 ± 3 | 20 |
| PMT-GFP/PMT-mRFP (negative) | 19 ± 9 | 19 ± 2 | 26 ± 3 | 24 |
| EGFR-GFP/EGFR–mRFP | 50 ± 25 | 50 ± 6 | 68 ± 8 | 18 |
| EGFR-GFP/mRFP-EGFR | 50 ± 25 | 50 ± 5 | 68 ± 7 | 21 |
| EGFR-GFP/EGFR-mRFP/wt EGFR (1:1:0.5)* | 44 ± 19 | 44 ± 5 | 60 ± 7 | 17 |
| EGFR-GFP/EGFR-mRFP/wt EGFR (1:1:1)* | 40 ± 18 | 40 ± 4 | 55 ± 5 | 22 |
| ErbB2-GFP/ErbB2-mRFP | 50 ± 26 | 50 ± 5 | 68 ± 7 | 24 |
| ErbB2-GFP/EGFR-mRFP | 62 ± 21 | 62 ± 4 | 85 ± 5 | 14 |
| mRFP-EGFR-GFP (positive) | 73 ± 15 | 73 ± 4 | 100 ± 6 | 14 |

*The ratio (1:1:0.5) was the ratio of amounts (mass) of plasmids used for transfection. So was the ratio of 1:1:1.

of the maximum intensity. $G_\infty$ is the convergence value of the autocorrelation function for long times, and in general this value is 1. $T$ is the average fraction of particles that reside in the triplet state and $\tau_T$ is its relaxation time. In some cases it was necessary to include two different triplet states to account for the photodynamics of FPs.

## FRET setup

Confocal laser scanning microscopy was performed on an LSM 510 META microscope (Carl Zeiss) with an oil immersion objective lens (63×, NA 1.4; Carl Zeiss). For sensitized fluorescence emission measurements, CFP and YFP were excited sequentially through an HFT 458/514 beam splitter by using 458 nm (30% laser intensity) and 514 nm (5% intensity) argon laser lines, respectively. Emission filters for the CFP channel (461–504 nm) and YFP channel (526–568 nm) were used, and FRET was detected through the FRET channel, in which fluorescence emission was monitored through the YFP channel upon excitation at 458 nm (donor excitation). As previously described (17,35), $FRET^C$ was calculated on a pixel-by-pixel basis for the entire ''region of interest (ROI)'' image by the equation: $FRET^C = FRET - (0.40 \times CFP) - (0.15 \times YFP)$, where FRET, CFP, and YFP correspond to background-subtracted fluorescence intensities acquired through the FRET, CFP, and YFP channels, respectively. The 0.4 and 0.15 are the fractions of bleed-through of CFP and YFP fluorescence to the FRET channel, respectively. The fractions were calculated by measuring fluorescence intensities of cells individually expressing EGFR-CFP or EGFR-YFP through the CFP, YFP, and FRET channels. $FRET^C$ was also normalized for both CFP and YFP intensities ($FRET^C / (C \times Y)^{1/2}$). All the experiments were done at room temperature (~22°C).

FRET spectra were obtained by scanning images from 462 to 612 nm in the META mode after exciting cells at 458 nm (30% laser intensity). After subtracting background fluorescence, fluorescence intensities were plotted against emission wavelengths, and were further normalized for intensities at 495 nm. Data are presented as the mean ±SD, and differences between groups were compared using Student's $t$-test (one-tailed).

# RESULTS AND DISCUSSION

## Calibration

A precondition for SW-FCCS is that fluorophores have to have similar excitation spectra but well-separated emission spectra (7,14). Due to the broad emission spectra of the FPs, cross talk in this system is unavoidable. In addition, cells possess an autofluorescence background that contributes differently to the two different channels. We thus first characterized every component according to their fluorescence characteristics. A laser power of 40 $\mu$W before the objective was chosen since at this level no obvious photobleaching could be observed in the fluorescence intensity traces or autocorrelation functions (ACFs). The following values are averages using an excitation wavelength of 514 nm and a laser power of 40 $\mu$W in our microscope settings:

$$\eta_g^G = 2000$$
$$\eta_r^G = 200$$
$$\eta_g^R = 0$$
$$\eta_r^R = 2000$$
$$\beta_g = 1800$$
$$\beta_r = 2800.$$

The position of FP, i.e., whether attached to the amino- or carboxyl-terminus, did have minimal influence on the count rate. However, cytosolic GFP (2400 cps) and mRFP (1500 cps) had somewhat different cps, and that of PMT-GFP and PMT-mRFP ranged between ~1100 and 2000 cps, and 800 and 2000 cps, respectively.

## Phosphorylation and internalization of receptor chimera with FP

It has been reported that activities of the chimeric receptor proteins are indistinguishable from the native proteins in terms of cell surface expression, and EGF-induced phosphorylation and internalization (30,36). Similar results are obtained here. When all the constructs were introduced into CHO cells, the chimeric proteins were expressed on the cell surface as shown in Fig. 1 *B*. When the EGFR constructs were introduced singly into COS-7 cells, which give higher protein expression levels compared to CHO cells, the chimeric receptor proteins were phosphorylated upon EGF binding (Fig. 2 *A*). When the cells were incubated with EGF (100 ng/ml), the chimeric EGFRs on the cell surface were efficiently internalized within 30 min or less except for chimeras with the amino-terminal fusion, mRFP-EGFR and mRFP-EGFR-GFP, whose internalization was slower than other EGFR constructs with carboxyl-terminal fusion and took up to 50 min for complete internalization (Fig. 2 *B*). This suggests that FP fusion with EGFR at its amino-terminus may affect the binding efficiency of the receptor for EGF. Nonetheless, the chimeric receptor mRFP-EGFR could form dimers with EGFR-GFP as efficiently as other combinations of chimeric receptors as shown in Table 1 and Fig. 3 *D*.

## Determination of receptor dimer fractions on the cell surface by SW-FCCS

To investigate if the cell-surface EGFR and ErbB2 have preformed homo- and heterodimeric structures, we set out to analyze the homo- and heterodimerization of EGFR and ErbB2 by SW-FCCS. CHO cells were transfected with plasmid constructs encoding EGFR or ErbB2 molecules fused to GFP or mRFP. FPs on the upper cell membrane of CHO cells were excited by a single laser line at 514 nm, and emissions were split by a dichroic mirror and were detected through two band-pass filters, one for GFP and the other for mRFP. Autocorrelation and cross-correlation curves of FPs fused to EGFR or ErbB2 expressed on the CHO cell surface were compared with those of FP fused to the PMT peptide as a negative control, in which FPs were attached to the PMT sequence (33) so that the FP chimeras are likely to be randomly distributed as monomers on the cytoplasmic membrane. All of the FP-fused EGFR or ErbB2 molecules laterally diffused with a similar diffusion coefficient, 0.38 ± 0.13 $\mu m^2/s$

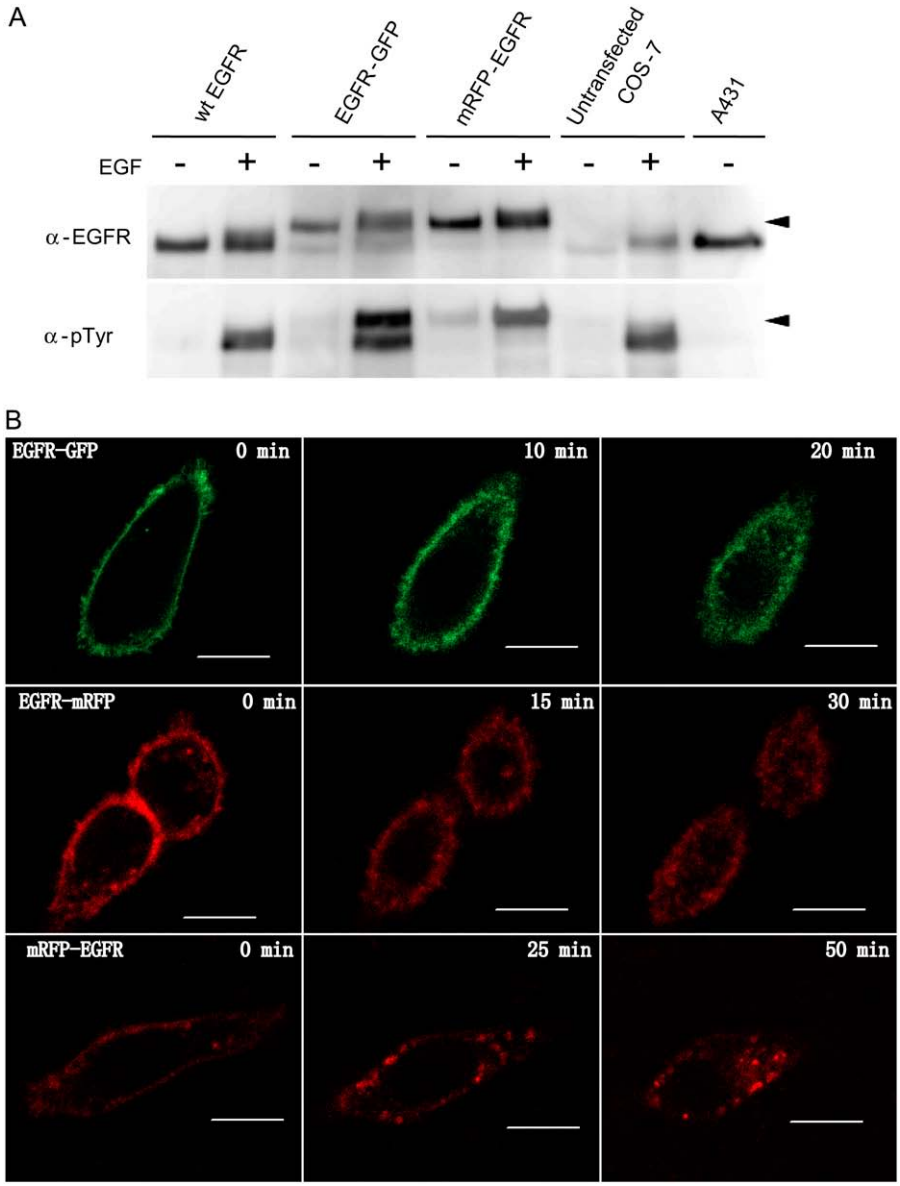


FIGURE 2 (*A*) Phosphorylation assay of FP-fused EGFR constructs. The chimeric constructs were introduced into COS-7 cells, and the cell lysates were prepared before (−) and after (+) stimulation with EGF. The lysates were blotted on filter membranes, and stained with anti-EGFR antibody ($\alpha$-EGFR) or anti-phosphotyrosine antibody ($\alpha$-pTyr). Note that COS-7 cells express the wild-type EGFR detectable by staining with the antibodies, particularly in the lanes of EGFR-GFP and untransfected COS-7. As a reference, a cell lysate of A431, which overexpresses the wild-type EGFR, was also included in the lane furthest to the right. Arrowheads indicate the positions of a molecular marker, 204-kDa myosin heavy chain. (*B*) FP-fusion EGFR internalization after EGF stimulation. (*Left*) Images before adding EGF; (*middle*) images show a certain scale of internalization after certain time of EGF stimulation; (*right*) images show large scale of internalization after longer time of EGF stimulation.

($n = 44$). The amplitudes of cross-correlation curves measured from cells coexpressing EGFR-GFP/mRFP-EGFR, ErbB2-GFP/EGFR-mRFP, or ErbB2-GFP/-mRFP were much higher than those expected for pure cross talk (Fig. 3, *D–G*), and in fact approaching the amplitude of cells expressing the positive control mRFP-EGFR-GFP (Fig. 3 *C*). The amplitude of cross-correlation curves of the negative controls, cells coexpressing cytosolic GFP/mRFP (Fig. 3 *A*) or PMT-GFP/-mRFP (Fig. 3 *B*), was similar to that due to cross talk. In all cases, cells were chosen that expressed the GFP and mRFP constructs in similar amounts to maximize the contribution to the cross correlation.

From the cross-correlation curves, the percentage of the receptor molecules found in homo- or heterodimers were calculated and summarized in Table 1. We never observed 100% cross correlation even for the positive control. One important reason may be that not all mRFP molecules function as fluorescent molecules, as reported by Hilleshein et al. (37). There also may be some other reasons, such as instability of the FPs against photobleaching and/or enzymatic degradation. With the average value of 73% dimerization measured in the positive control, SW-FCCS suffers from a problem similar to the zero-efficiency peak observed in FRET (38), which is caused by the absence of the acceptor on a subpopulation of molecules. However, in the case of SW-FCCS this problem is more severe since both the absence of a GFP as well as the absence of an mRFP molecule would lead to a reduced value of dimer formation. When comparing the standard deviation of the positive control and the other experiments it is evident that the positive control shows a much smaller standard deviation. This can be explained by the fact that in this case only FP stability

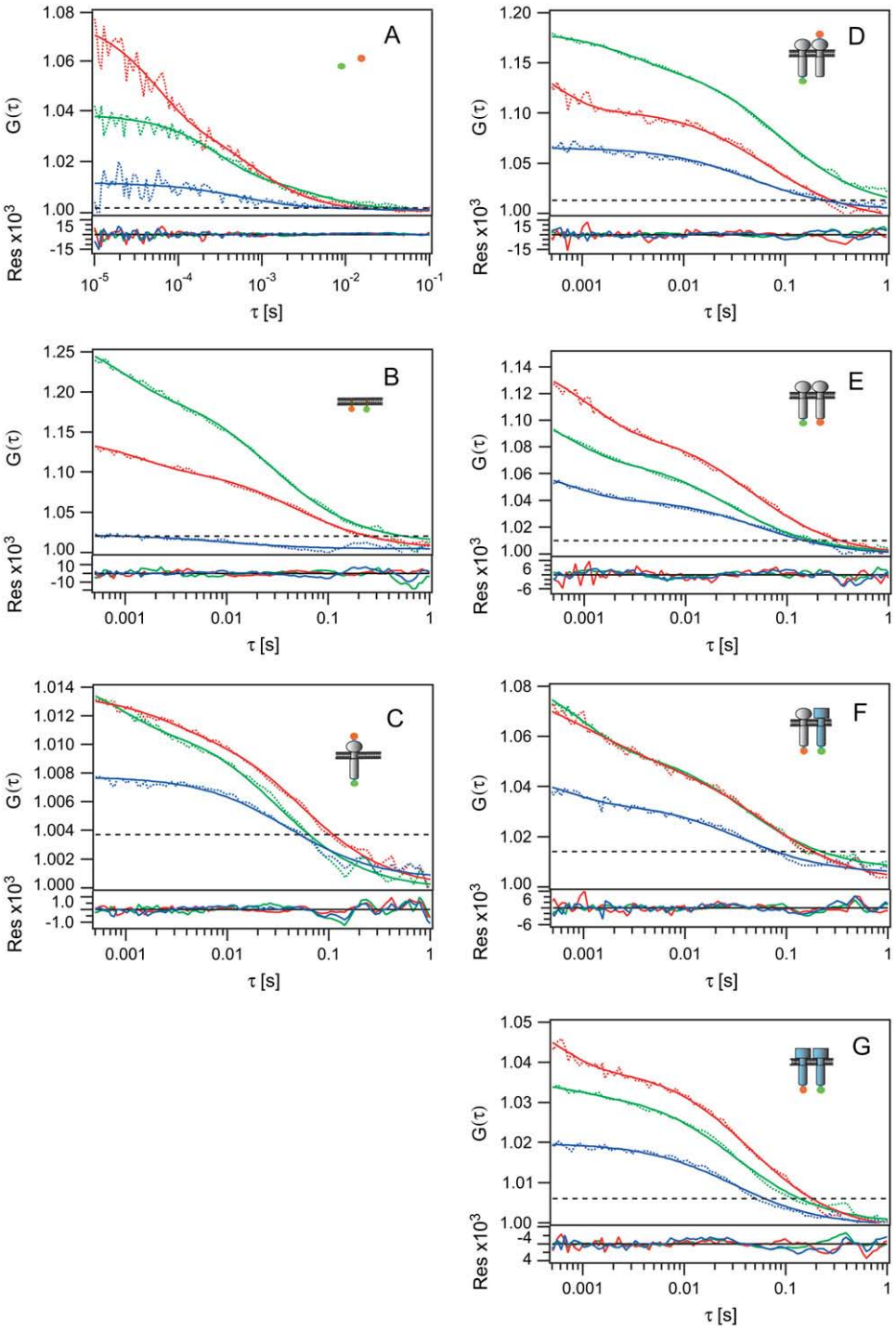


FIGURE 3 Auto- and cross-correlation curves measured from CHO cells expressing chimeric FPs. Autocorrelation curves (*dashed curves*) of GFP (*green*) and mRFP (*red*), and cross-correlation curves (*blue*) between the two are shown with their fits (*solid curves*). Black dotted lines represent cross-correlation levels due to cross talk between the two channels. (*A*) Cell coexpressing cytosolic free GFP and mRFP (negative control 1). (*B*) PMT-GFP/-mRFP (negative control 2). No cross correlation, hence no interaction, between the two FPs was observed. (*C*) Cell expressing mRFP-EGFR-GFP (positive control), in which mRFP and GFP were fused in tandem to N- and C-termini of EGFR, respectively. (*D*) Cell coexpressing EGFR-GFP/mRFP-EGFR. Similar auto- and cross-correlation curves were also observed for cells co-expressing EGFR-GFP/-mRFP (*E*). (*F*) Cell coexpressing ErbB2-GFP/EGFR-mRFP. (*G*) Cell coexpressing ErbB2-GFP/-mRFP.

determines the fraction of double-labeled complexes observed and there is no influence of any other biological factors on actual complexation between the two fluorophores. This upper limit of observable dimerization, caused by artifacts of the FP stability, leads to an underestimation of the actual dimer fraction and these values therefore constitute a lower limit of dimerization. We give in Table 1 also the dimer fractions normalized to the average value of 73% observed in the positive control to show the upper limit of dimerization. The dimer percentages observed for the homo- and heterodimers were significantly higher ($P \leq 0.001$) than that for the negative control. All the three dimer percentages were similar to one another, and might not be significantly different ($P > 0.05$), indicating that the majority of the receptor molecules have dimeric structures on the cell surface. These dimer percentages were not affected by the

receptor expression levels ranging from $2.0 \times 10^4$ to $2.6 \times 10^5$ molecules per cell (Fig. 4). This indicates that the receptor homo- and heterodimerization are not dependent on receptor expression levels, as previously observed for EGFR homodimerization (24).

To further confirm the dimer faction of the receptors obtained from SW-FCCS, a third unlabeled receptor was introduced to the coexpression system of FP-fusion receptors (i.e., EGFR-GFP/EGFR-mRFP) by adding a third wt EGFR plasmid (pNUT/EGFR) in transfection. The third wt EGFR would compete with the dimer formation between EGFR-GFP and EGFR-mRFP, thus a decrease of dimer fraction should be observed. This is shown in Table 1 with two sets of triple-transfection data. The dimer faction of EGFR-GFP/EGFR-mRFP decreases with the increase of the amount of the third plasmid. With the increase of the ratio of EGFR-GFP/EGFR-mRFP/wt EGFR from 1:1:0.5 to 1:1:1, the dimer faction drops from 44% to 40%, and both are lower than that of the coexpression of EGFR-GFP/EGFR-mRFP (50%). Note that the ratio was the mass ratio of different plasmids and the molar ratio may be different (which depends on the vector size). Besides, each individual cell may take in different amounts of the plasmids. As the third unlabeled receptor is not detectable in SW-FCCS and the concentration of wt EGFR may differ from cell to cell, the competition effect may differ from that estimated by the plasmid ratio. However, the averaged values of the dimer fraction from different sets of cell samples can still indicate the competition effect, which confirms that SW-FCCS is applicable to study protein-protein interactions in live cells.

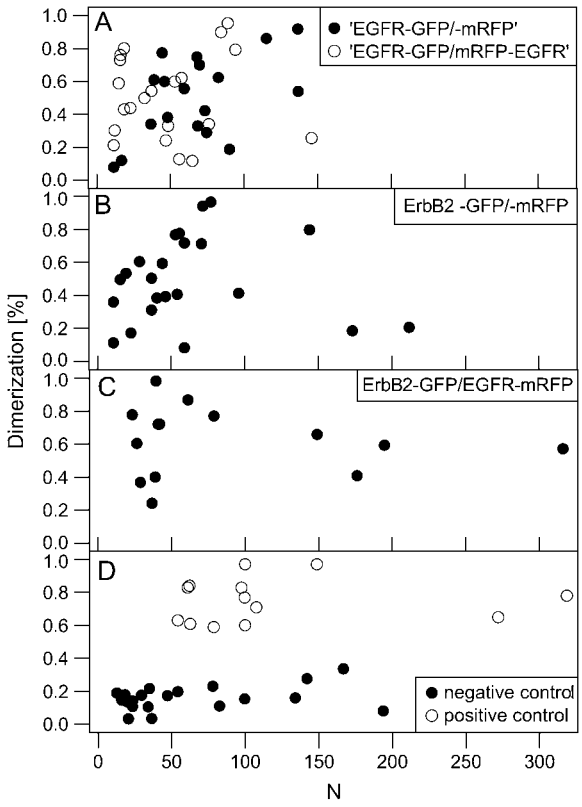


FIGURE 4 Dimerization percentages versus receptor expression level. (*A*) Coexpression of EGFR-GFP/EGFR-mRFP, and coexpression of EGFR-GFP/mRFP-EGFR. (*B*) Coexpression of ErbB2-GFP/ErbB2-mRFP. (*C*) Coexpression of EGFR-GFP/ErbB2-mRFP. (*D*) Positive control mRFP-EGFR-GFP, and negative control coexpression of PMT-GFP/PMT-mRFP.

The dimer fractions of the receptors obtained from SW-FCCS, which were done at room temperature (RT), are comparable with the chemical cross-linking results reported by Moriki et al., which were done at 37°C (24). Thus we assume that there is little influence on dimer formation between 37°C and RT. Similar to the report by Bacia et al. where they discussed the advantages of FCS done at RT (39), here we performed SW-FCCS at RT considering the photostability of FPs and slower endocytosis rate of membrane receptors at RT than at higher temperature.

## SW-FCCS on cells after EGF stimulation

After EGF stimulation the ACF and cross-correlation function (CCF) curves on the membrane undergo dramatic changes. When focusing on a single position on a cell directly after stimulation the process during receptor activation can be detected. Fig. 5 shows the observation of clustering of EGFR-GFP and EGFR-mRFP by SW-FCCS. In the first minutes changes are small and the ACF and CCF curves are similar to the state before EGF stimulation (Fig. 5, *A* and *B*). After a longer time of ~10 min after stimulation, irregular high intensity fluorescence peaks are detected, consistent with receptor clustering on the membrane (Fig. 5, *C* and *D*). The observation of EGFR receptor clusters on membrane after activation is consistent with the report by Lakadamyali et al. (40), which implies that SW-FCCS may be applied to monitor receptor activation in vivo.

## Stability of the mathematical determination of the dimer fraction

From the different count rates detected for cytosolic and membrane-targeted FPs, it is clear that under the experimental conditions used, the cps of the FPs can range between ~1000 and 2000 counts. In particular, the cps depends on how well the focal volume is focused on the membrane (41). These variations could affect the calculation of the dimer fractions. Thus we calculated the dimer fractions assuming the lower range of cps of $\eta_g^G = 1100$, $\eta_r^G = 100$, $\eta_g^R = 0$, and $\eta_r^R = 800$ but assuming the same background count rates as above. However, the dimer fraction determined did not change significantly in any of the cases. The fraction of dimers determined depends on individual values for the fluorescence yield and background. However, when all the values were changed by the same factor, as would happen in a limited range when changing the laser intensity or defocusing from the membrane, the dimer fraction determined

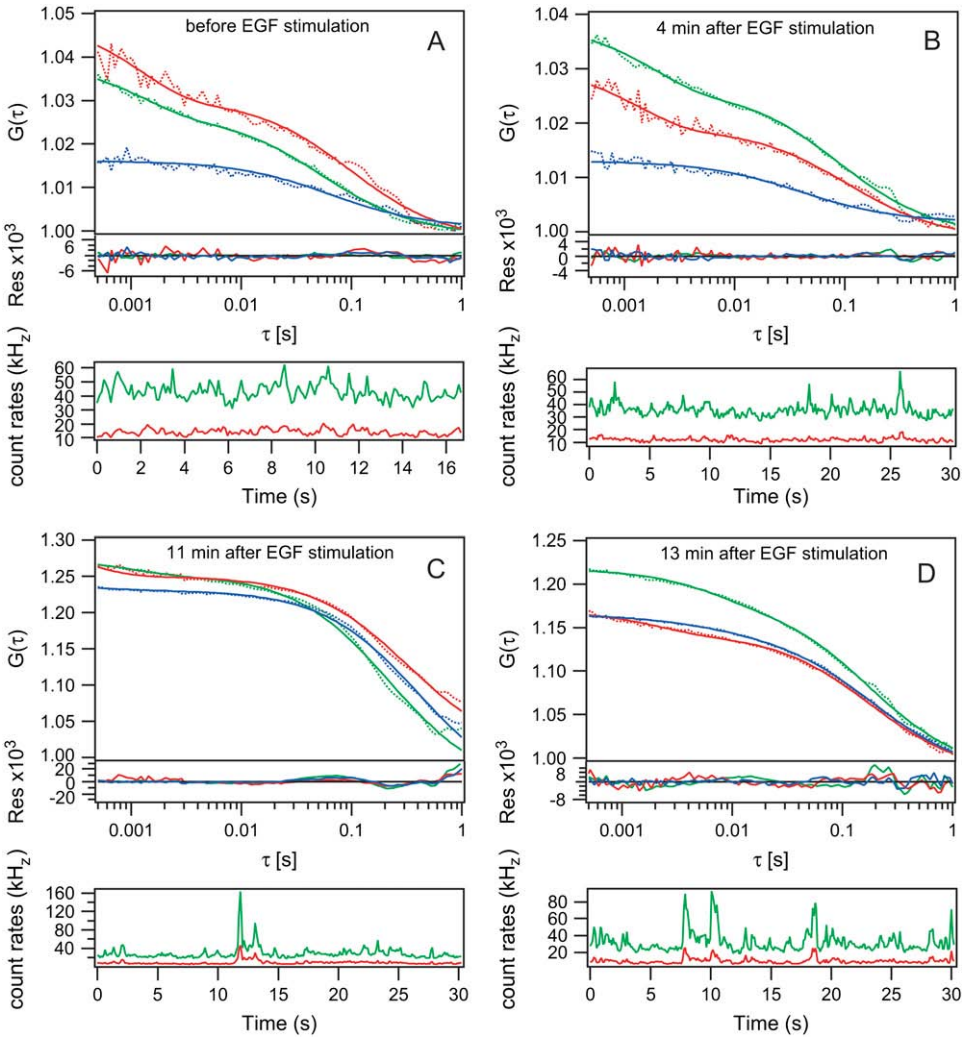


FIGURE 5 Auto- and cross-correlation curves measured from one CHO cell expressing EGFR-GFP/EGFR-mRFP before and after ligand stimulation. (*A*) ACF and CCF curves before adding EGF. (*B*, *C*, and *D*) 4 min, 11 min, and 13 min after EGF stimulation, respectively.

was almost unchanged. Thus, although focusing on the membrane and laser intensity changes can be problems in FCS and FCCS (41), the influence of these effects on the dimer fraction is small. A simultaneous change of all fluorescence yields and background values by a factor of 2 up or down did change the dimer fractions determined by $<2$ percentage points, far smaller than the standard deviation. The exception was the PMT-GFP/-mRFP negative control, which gave larger values as discussed in the next section. Thus the determination of the homo- and heterodimer fraction is stable and does not vary strongly with changes in cps.

## Negative controls and errors

The lower limit of dimer formation in the negative controls is probably due to the fact that the background values used in our calculations are average values over many cells. However, every cell will exhibit a different background value that cannot be assessed independently from the expressed FPs. Thus there is an uncertainty in the values for the background ($\beta$) and the fluorescence yield ($\eta$), which limits the accuracy of the measurement and explains as well the large errors in the dimer fraction. In addition, it should be noted that for the PMT-GFP/-mRFP measurements the correlation times for the cross correlations do not agree with those of the autocorrelations in many cases and often the cross correlations could not be fit at all. This is very different from all the other measurements where the correlation times of cross correlations and autocorrelations do agree. This clearly indicates that there is limited cross correlation seen in the case of the negative controls PMT-GFP/-mRFP and free GFP/mRFP expressed in the cytoplasm.

To confirm the measurements presented above, we depict the typical intensity traces for the positive and negative controls as well as for the EGFR-GFP/mRFP-EGFR coexpression (Fig. 6). Although in the positive control the signal in the two different detection channels is strongly correlated, in the negative control this is not the case. In the case of EGFR-GFP/mRFP-EGFR coexpression the intensity traces show correlations, but there are as well intensity peaks appearing

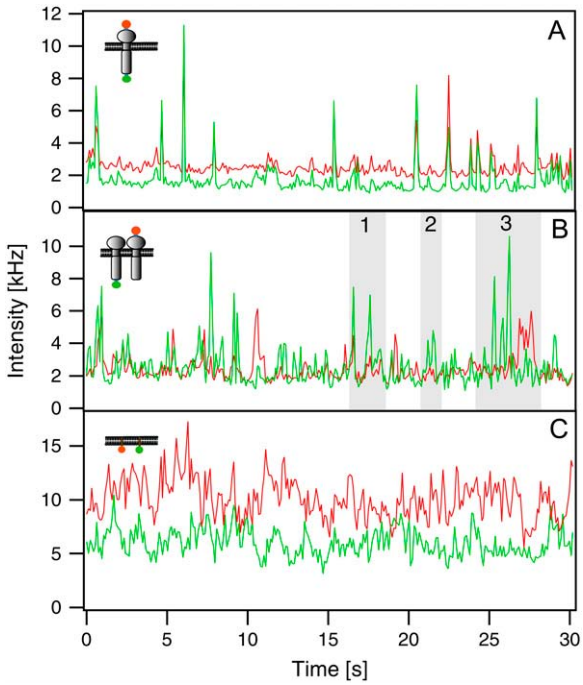


FIGURE 6 Intensity traces of positive and negative controls, and EGFR-GFP/mRFP-EGFR. The long wavelength channel (mRFP) is depicted in red, and the short wavelength channel (GFP) in green. (*A*) The positive control shows that peaks in the red and green channels appear mainly simultaneously as expected. (*B*) For the EGFR-GFP/mRFP-EGFR coexpression, some peaks are correlated (*shaded area 1*), some are most likely due to cross talk (*shaded area 2*), and some are uncorrelated (*shaded area 3*). (*C*) In the negative control the signals in the two channels are uncorrelated except some residual correlation due to cross talk.

only in either the red or the green channel. These uncorrelated peaks could be due to either EGFR-GFP/-GFP and mRFP-EGFR/-EGFR dimers or to monomeric forms of these proteins.

## Influence of FRET between GFP and mRFP on the calculated dimer fraction

As reported in the next section we detected FRET between EGFR-CFP and -YFP coexpressed in CHO cells. GFP and mRFP are reported to have a similar Förster distance as CFP/YFP of ~4.7 nm (42), and thus it is important to determine whether there is any FRET between EGFR-GFP and -mRFP. This would influence the fluorescence yield values $\eta$ and thus the calculated dimer fractions. To test whether there is any FRET and if it has any influence on our results, we coexpressed EGFR-GFP with either EGFR-mRFP or mRFP-EGFR, where mRFP is attached to either the -carboxyl or the amino-terminus. Coexpression of the constructs leads then to a situation where GFP and mRFP are either both on the cytoplasmic side (Fig. 3 *E*) and are possibly in close contact (similar to the EGFR-CFP/-YFP situation), or where GFP is on the cytoplasmic side and mRFP on the extracellular side of the membrane (Fig. 3 *D*), at a larger distance from each other.

As can be seen from Fig. 3, *D* and *E*, and Table 1, the measured cross correlation and calculated fraction of dimers is the same for both situations. We thus conclude that there is either no FRET or no significant influence of FRET on our measurements. This is probably due to the fact that mRFP has a long excitation tail on the short wavelength side, which allows direct excitation of mRFP by the 514 nm line of the laser and makes it a bad FRET acceptor (15). Furthermore, the excitation of GFP at 514 nm is reduced so that the direct excitation of mRFP largely dominates compared to FRET from GFP to mRFP. This is in agreement with the work of Saito et al., who have not found any FRET in a GFP/mRFP pair linked by the D4K linker (1).

Incidentally, this experiment demonstrates as well that a dimerization due to the interaction between FPs can be excluded since for the EGFR-GFP/mRFP-EGFR the FPs reside on different sides of the membrane.

## FRET-based observation of receptor dimers on the surface of live cells

To further confirm the preformed dimeric structures of the receptors, we also tried to detect FRET between FPs fused to the receptor molecules. CHO cells were cotransfected with the FP-fused receptor constructs by electroporation, and cells expressing $\sim 5 \times 10^4$ molecules per cell, with the ratios of YFP/CFP ranging from one to three, were selected based on their fluorescence intensities (Fig. 7). CHO cells have an advantage of no endogenous expression of EGFR family members except for a low background expression of ErbB2, considering that very few cell lines express EGFR in the absence of ErbB2 (43,44). The fluorescence intensities of CFP-, YFP-tagged chimeric receptors were measured through three filter sets (CFP, YFP, and FRET channels); corrected FRET values ($FRET^C$) were calculated according to a previously published method (17,36), whereby fluorescence intensity measured through the FRET channel was corrected for cross talk between the channels. Examples of such $FRET^C$ are shown in Table 2. All the $FRET^C$ intensities between EGFR-CFP and -YFP, ErbB2-CFP and -YFP, and ErbB2-CFP and EGFR-YFP were statistically significantly higher ($P < 0.001$) than that of the negative control PMT-CFP/-YFP, whereas they were lower than that of the positive control PMT-CFP-YFP, in which FPs were tandemly fused to PMT. These results summarized in Table 2, in which $FRET^C$ intensities were normalized for intensities of CFP and YFP as described previously (45), suggest that EGFR and ErbB2 are able to preform homo- and heterodimers without bound ligand on the cell surface at physiological expression levels.

To verify the FRET results above, we also tried to detect a fluorescence intensity increase of YFP due to FRET as previously shown (45,46). CHO cells were cotransfected

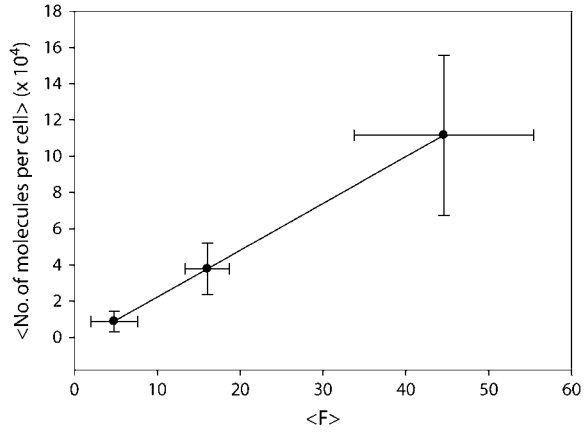


FIGURE 7 Standard curve for the calculation of the number of receptor molecules expressed on the cell surface from fluorescence intensities. Confocal images of CHO cells expressing EGFR fused to YFP at low, medium, and high levels were obtained, and fluorescence intensities of ROI with a fixed size were measured. The same populations of the cells were also observed by FCS to measure the number of the receptor molecules in the confocal volume, from which the number of the receptor molecules per cell was calculated using 0.196 $\mu m^2$ of the membrane area in the confocal volume and 482 $\mu m^2$ as the average surface area of CHO cells. For this calculation, we assumed that particles detected by FCS consist of two receptor molecules (dimer). The number of molecules of CFP was also similarly estimated from its fluorescence intensity based upon the fluorescence intensity ratio, 0.22, of CFP/YFP under the experimental conditions used. The ratio was determined by measuring fluorescence intensities of cells expressing CFP-EGFR-YFP or YFP-EGFR-CFP, in which CFP and YFP were fused to the amino- and carboxyl termini under the same experimental conditions. ''No. of molecules per cell'' and ''F'' represent the mean number of molecules per cell and the mean fluorescence intensity of ROI, respectively. Data points are the mean ± SD of more than six cells.

with chimeric constructs between the receptor, EGFR or ErbB2, and FP, CFP, or YFP. Cells transiently expressing the chimeric proteins on the cell surface at physiological levels were selected based on fluorescence intensities, and emission wavelength scans were performed in the range of 462–612 nm with the excitation wavelength of 458 nm. If CFP and YFP were in close proximity due to homo- or heterodimerization of the receptors, higher peaks at 537 nm (YFP emission due to FRET) should be observed after normalization of the spectra to fluorescence intensities at an emission wavelength of 494 nm (CFP emission) than that of the negative control. As shown in Fig. 8, *A–C*, indeed, spectral peaks at 537 nm of cells coexpressing EGFR-CFP/-YFP, ErbB2-CFP/-YFP, and ErbB2-CFP/EGFR-YFP were statistically significantly higher ($P < 0.001$) than that of the negative control PMT-CFP/-YFP, but lower than that of the positive control PMT-CFP-YFP. A similar spectrum to that of ErbB2-CFP/EGFR-YFP was also obtained for cells coexpressing EGFR-CFP/ErbB2-YFP (Fig. 8 *D*).

**TABLE 2 FRET between FPs fused to EGFR and ErbB2 on the cell surface**

| Construct | $FRET^C/\sqrt{(C*Y)}$ (± SD) | No. of molecules/cell* (± SD) | Sample size (*n*) |
|---|---|---|---|
| PMT-CFP/-YFP (negative) | 0.036 ± 0.026 | 66,000 ± 17,000 | 38 |
| EGFR-CFP/-YFP | 0.103 ± 0.040 | 56,000 ± 22,000 | 31 |
| ErbB2-CFP/-YFP | 0.078 ± 0.038 | 61,000 ± 21,000 | 17 |
| EGFR-CFP/ErbB2-YFP | 0.157 ± 0.077 | 37,000 ± 14,000 | 18 |
| ErbB2-CFP/EGFR-YFP | 0.179 ± 0.086 | 43,000 ± 22,000 | 23 |
| PMT-CFP-YFP (positive) | 0.476 ± 0.083 | 52,000 ± 23,000 | 35 |

## Comparison between FRET and SW-FCCS data

FRET data was used in this work to confirm the interaction between the protein constructs and thus as a support for the SW-FCCS data. Although FRET data indicated that EGFR and ErbB2 form homo- and heterodimers, the transfer efficiency found is low. This is consistent with other work on FRET of fluorescent proteins in which FRET for CFP/YFP constructs with a distance of ~52 Å show a FRET efficiency of only 33% (47) consistent with a Förster radius of 47.5 Å (42). The distance between the kinase domains of EGFR dimers is ~50 Å (48). Taking this as an average distance for the C-terminal FPs we would expect a FRET efficiency of 42% or less as seen in our measurements. SW-FCCS measurements confirm the interaction and allow quantification of the dimer formation on the cell surface. From the measured average values and standard deviations we suggest that the majority of EGFR and ErbB2 receptors are found in homo- and heterodimers before activation, whereas the exact amount of dimerization can vary from point to point on a cell.

The aim of this work was to test whether preformed dimers exist on the cell surface before EGF stimulation. We thus used a mathematical model allowing only for the presence of monomers and dimers with the result that preformed dimers are a prevalent form on the cell surface consistent with models suggested in literature (24,28,30). However, we cannot categorically exclude the presence of larger preformed oligomers on the cell surface although we did not observe intensity peaks consistent with larger oligomers or aggregates before stimulation (Fig. 6). If they exist, their presence would change the relative fractions of monomers and oligomers as determined in this work. Experiments after EGF stimulation, in contrast, show larger aggregates appearing on the cell surface, and show internalization and phosphorylation of the proteins similar to wild-type EGFR consistent with the detection of higher order oligomers after activation reported in literature (30).

## CONCLUSIONS

In this work we developed a novel quantitative method to detect protein-protein interactions in vivo to assess the dimerization properties of EGFR and ErbB2. Single wavelength excitation fluorescence cross-correlation spectroscopy overcomes the difficulty of aligning two laser lines to overlap

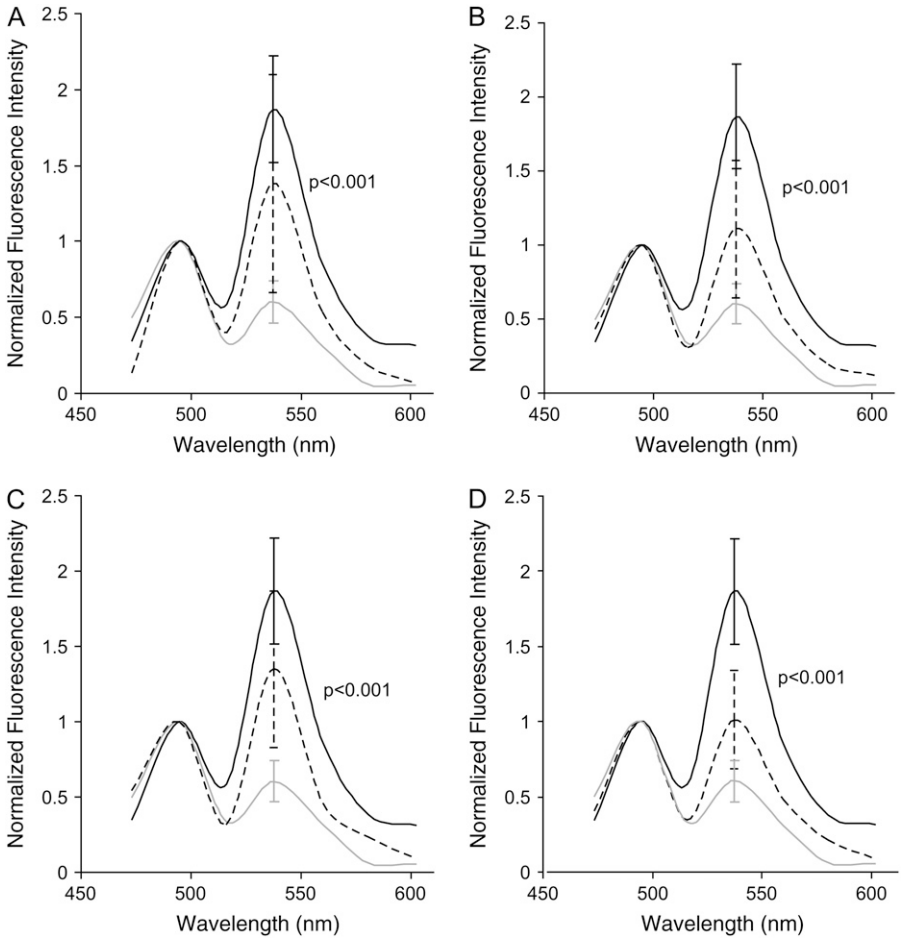


FIGURE 8 Preformed homo- and heterodimers of EGFR and ErbB2 detected by FRET on the live cell surface. Fluorescence spectra (*dashed line*) were measured on live CHO cells coexpressing EGFR-CFP/-YFP (*A*), ErbB2-CFP/-YFP (*B*), ErbB2-CFP/EGFR-YFP (*C*), and EGFR-CFP/ErbB2-YFP (*D*) by confocal microscopy, and were normalized for fluorescence intensities at 498 nm. Spectra of the positive (*black line*) and negative (*gray line*) controls, and *P*-values between fluorescence intensities of cells expressing the chimeric receptors and the negative control are also shown.

each other for dual-laser excitation and instead uses a single laser line for the one-photon excitation of two fluorophores with similar excitation characteristics but separable emission spectra. In this case GFP and mRFP were chosen as fluorescent labels since their photocharacteristics make them an ideal pair for SW-FCCS at 514 nm excitation. First, the emission spectra of GFP and mRFP are well separated and both FPs are more photostable, compared to the CFP/YFP pair. Second, the absorption peak around 510 nm of mRFP (42) gives sufficient red signal for excitation at 514 nm and the excitation of GFP not at its excitation maximum results in comparable signals in both channels with minimum cross talk, which is confirmed by quantitative analysis on positive and negative controls.

Crystal structures of the extracellular domain of EGFR suggest that ligand binding releases the intramolecular tether, and makes the ''dimerization'' arm available for intermolecular interaction of two extracellular domains of the receptor molecules (49–51). Furthermore, crystal structures of the extracellular domain of ErbB2 have revealed that it has an untethered structure, and resembles the ligand-bound form of EGFR (52,53). The receptor homo- and heterodimers on the cell surface may be able to take two major structures, one with an intramolecular tether, which is similar to ligand-unbound EGFR, and the other with an untethered structure like ErbB2. These two structures may correspond to the receptors on the cell surface, which have low and high affinities for EGF, respectively, as discussed previously (23). Indeed, weakening of the intramolecular tether by mutations increases the proportion of high affinity sites, and strengthening of the tether abolishes high affinity binding (54). Coexpression of ErbB2 with EGFR increases the fraction of high-affinity receptors without alteration of the total number of EGF binding sites per cell (55). This suggests the intermolecular interaction between EGFR and ErbB2 before ligand binding, and is consistent with the preformed heterodimeric structure demonstrated by this work. The untethered ''dimerization'' arm of ErbB2 may transiently interact with that of EGFR in the heterodimeric structure, resulting in the increase in the population of high-affinity receptors.

Using SW-FCCS we have demonstrated that members of the EGFR family receptors at physiological expression levels have preformed homo- and heterodimeric structures on the cell surface. These findings are supported as well by other recent publications (30,56) and are, indeed, consistent with the homodimeric structures of the EGFR kinase domain (57),

transmembrane domain (58), and unactivated extracellular domain (51) that have previously been determined. Ligand-induced intermolecular interaction of the two ''dimerization'' arms in the homo- and heterodimers may also induce the rotation/twist of the transmembrane domains of the receptor dimers, and may result in dissociation of the dimeric kinase domains for receptor activation (24). The dissociated kinase may phosphorylate tyrosine residues in the receptor's regulatory domain and other substrates through allosteric activation by asymmetric kinase domain dimers as recently demonstrated (48). When inhibitors against the receptor kinase are developed as anticancer drugs, the preformed homo- and heterodimeric structures of the receptors should be considered because they may dissociate the dimeric cytoplasmic kinase domains (24,57). These homo- and heterodimeric structures of EGFR and ErbB2 raise the possibility of new anticancer drugs acting at the receptor dimer interface.

The authors thank R. Tsien and H. Wang for plasmids encoding mRFP and ErbB2, respectively. The authors gratefully acknowledge H. Miyagi for his technical support on the phosphorylation assay of FP-fusion receptor constructs.

This work was supported in part by a Research Grant of the Academic Research Fund of the Ministry of Education to T.W. and I.N.M. and a grant from the Singapore Bioimaging Consortium (SBIC 003/2005) to T.W. and S.A. P.L. is a recipient of a graduate scholarship from the National University of Singapore.

## REFERENCES

1. Saito, K., I. Wada, M. Tamura, and M. Kinjo. 2004. Direct detection of caspase-3 activation in single live cells by cross-correlation analysis. *Biochem. Biophys. Res. Commun.* 324:849–854.
2. Magde, D., E. Elson, and W. W. Webb. 1972. Thermodynamic fluctuations in a reacting system-measurement by fluorescence correlation spectroscopy. *Phys. Rev. Lett.* 29:705–708.
3. Schwille, P., F. J. Meyer-Almes, and R. Rigler. 1997. Dual-color fluorescence cross-correlation spectroscopy for multicomponent diffusional analysis in solution. *Biophys. J.* 72:1878–1886.
4. Schwille, P. 2001. Cross-Correlation Analysis in FCS. *In* Fluorescence Correlation Spectroscopy: Theory and Applications. E. L. Elson and R. Rigler, editors. Springer, Berlin, Germany. 360–378.
5. Weidemann, T., M. Wachsmuth, M. Tewes, K. Rippe, and J. Langowski. 2002. Analysis of ligand binding by two-colour fluorescence cross-correlation spectroscopy. *Single Mol.* 3:49–61.
6. Heinze, K. G., A. Koltermann, and P. Schwille. 2000. Simultaneous two-photon excitation of distinct labels for dual-color fluorescence cross-correlation analysis. *Proc. Natl. Acad. Sci. USA.* 97:10377–10382.
7. Bacia, K., S. A. Kim, and P. Schwille. 2006. Fluorescence cross-correlation spectroscopy in living cells. *Nat. Methods.* 3:83–89.
8. Kogure, T., S. Karasawa, T. Araki, K. Saito, M. Kinjo, and A. Miyawaki. 2006. A fluorescent variant of a protein from the stony coral *Montipora* facilitates dual-color single-laser fluorescence cross-correlation spectrsocopy. *Nat. Biotechnol.* 24:577–581.
9. Stoevesandt, O., K. Köhler, R. Fischer, I. C. Johnston, and R. Brock. 2005. One-step analysis of protein complexes in microliters of cell lysate. *Nat. Methods.* 2:833–835.
10. Thompson, N. L., A. M. Lieto, and N. W. Allen. 2002. Recent advances in fluorescence correlation spectroscopy. *Curr. Opin. Struct. Biol.* 12:634–641.
11. Krichevsky, O., and G. Bonnet. 2002. Fluorescence correlation spectroscopy: the technique and its applications. *Rep. Prog. Phys.* 65:251–297.
12. Rička, J., and Th. Binkert. 1989. Direct measurement of a distinct correlation function by fluorescence cross correlation. *Phys. Rev. A.* 39:2646–2652.
13. Hwang, L. C., and T. Wohland. 2005. Single wavelength excitation fluorescence cross-correlation spectroscopy with spectrally similar fluorophores: resolution for binding studies. *J. Chem. Phys.* 122:114708.
14. Hwang, L. C., and T. Wohland. 2004. Dual-color fluorescence cross-correlation spectroscopy using single laser wavelength excitation. *ChemPhysChem.* 5:549–551.
15. Hwang, L. C., M. Gösch, T. Lasser, and T. Wohland. 2006. Simultaneous multicolor fluorescence cross-correlation spectroscopy to detect higher order molecular interactions using single wavelength laser excitation. *Biophys. J.* 91:715–727.
16. Campbell, R. E., O. Tour, A. E. Palmer, P. A. Steinbach, G. S. Baird, D. A. Zacharias, and R. Y. Tsien. 2002. A monomeric red fluorescent protein. *Proc. Natl. Acad. Sci. USA.* 99:7877–7882.
17. Gordon, G. W., G. Berry, X. H. Liang, B. Levine, and B. Herman. 1998. Quantitative fluorescence resonance energy transfer measurements using fluorescence microscopy. *Biophys. J.* 74:2702–2713.
18. Woolhead, C. A., P. J. McCormick, and A. E. Johnson. 2004. Nascent membrane and secretory proteins differ in FRET-detected folding far inside the ribosome and in their exposure to ribosomal proteins. *Cell.* 116:725–736.
19. Lackowicz, J. R. 1999. Energy transfer. *In* Principles of Fluorescence Spectroscopy, 2nd Ed. Plenum, New York. 367–394.
20. Shaner, N. C., P. A. Steinbach, and R. Y. Tsien. 2005. A guide to choosing fluorescent proteins. *Nat. Methods.* 12:905–909.
21. Mendelsohn, J., and J. Baselga. 2000. The EGF receptor family as targets for cancer therapy. *Oncogene.* 19:6550–6565.
22. Schlessinger, J. 2002. Ligand-induced, receptor-mediated dimerization and activation of EGF receptor. *Cell.* 110:669–672.
23. Burgess, A. W., H.-S. Cho, C. Eigenbrot, K. M. Ferguson, T. P. J. Garrett, D. J. Leahy, M. A. Lemmon, M. X. Slikowski, C. W. Ward, and S. Yokoyama. 2003. An open-and-shut case? Recent insights into the activation of EGF/ErbB receptors. *Mol. Cell.* 12:541–552.
24. Moriki, T., H. Maruyama, and I. N. Maruyama. 2001. Activation of preformed EGF receptor dimers by ligand-induced rotation of the transmembrane domain. *J. Mol. Biol.* 311:1011–1026.
25. Martin-Fernandez, M., D. T. Clarke, M. J. Tobin, S. V. Jones, and G. R. Jones. 2002. Preformed oligomeric epidermal growth factor receptors undergo an ectodomain structure change during signaling. *Biophys. J.* 82:2415–2427.
26. Gadella, T. W. Jr., and T. M. Jovin. 1995. Oligomerization of epidermal growth factor receptors on A431 cells studied by time-resolved fluorescence imaging microscopy. A stereochemical model for tyrosine kinase receptor activation. *J. Cell Biol.* 129:1543–1558.
27. Sako, Y., S. Minoguchi, and T. Yanagida. 2000. Single-molecule imaging of EGFR signaling on the surface of living cells. *Nat. Cell Biol.* 2:168–172.
28. Yu, X., K. D. Sharma, T. Takahashi, R. Iwamoto, and E. Mekada. 2002. Ligand-independent dimer formation of epidermal growth factor receptor (EGFR) is a step separable from ligand-induced EGFR signaling. *Mol. Biol. Cell.* 13:2547–2557.
29. Canals, F. 1992. Signal transmission by epidermal growth factor receptor: coincidence of activation and dimerization. *Biochemistry.* 31:4493–4501.
30. Clayton, A. H. A., F. Walker, S. G. Ochard, C. Henderson, D. Fuchs, J. Rothacker, E. C. Nice, and A. W. Burgess. 2005. Ligand-induced dimer-tetramer transition during the activation of the cell surface epidermal growth factor receptor-a multidimensional microscopy analysis. *J. Biol. Chem.* 280:30392–30399.
31. Pramanik, A., and R. Rigler. 2001. Ligand-receptor interactions in the membrane of cultured cells monitored by fluorescence correlation spectroscopy. *Biol. Chem.* 382:371–378.
32. Orr, G., D. Hu, S. Özçelik, L. K. Opresko, H. S. Wiley, and S. D. Colson. 2005. Cholesterol dictates the freedom of EGF receptors and HER2 in the plane of the membrane. *Biophys. J.* 89:1362–1373.

33. Chapple, J. P., A. J. Hardcastle, C. Grayson, K. R. Willison, and M. E. Cheetham. 2002. Delineation of the plasma membrane targeting domain of the X-linked retinitis pigmentosa protein RP2. *Invest. Ophthalmol. Vis. Sci.* 43:2015–2020.

34. Ho, S. N., H. D. Hunt, R. M. Horton, J. K. Pullen, and L. R. Pease. 1989. Site-directed mutagenesis by overlap extension using the polymerase chain reaction. *Gene*. 77:51–59.

35. Youvan, D. C., W. J. Coleman, C. M. Silva, J. Petersen, E. J. Bylina, and M. M. Yang. 1997. Fluorescence imaging micro-spectrophotometer (FIMS). *Biotechnol. Alia.* 1:1–16.

36. Carter, R. E., and A. Sorkin. 1998. Endocytosis of functional epidermal growth factor receptor-green fluorescent protein chimera. *J. Biol. Chem.* 273:35000–35007.

37. Hillesheim, L. N., Y. Chen, and J. D. Muller. 2006. Dual-color photon counting histogram analysis of mRFP1 and EGFP in living cells. *Biophys. J.* 91:4273–4284.

38. Deniz, A. A., M. Dahan, J. R. Grunwell, T. Ha, A. E. Faulhaber, D. S. Chemla, S. Weiss, and P. G. Schultz. 1999. Single-pair fluorescence resonance energy transfer on freely diffusing molecules: observation of Förster distance dependence and subpopulations. *Proc. Natl. Acad. Sci. USA*. 96:3670–3675.

39. Bacia, K., D. Scherfeld, N. Kahya, and P. Schwille. 2004. Fluorescence correlation spectroscopy relates rafts in model and native membranes. *Biophys. J.* 87:1034–1043.

40. Lakadamyali, M., M. J. Rust, and X. Zhuang. 2006. Ligands for clathrin-mediated endocytosis are differentially sorted into distinct populations of early endosomes. *Cell.* 124:997–1009.

41. Milon, S., R. Hovius, H. Vogel, and T. Wohland. 2003. Factors influencing fluorescence correlation spectroscopy measurements on membranes: simulations and experiments. *Chem. Phys.* 288:171–186.

42. Peter, M., S. M. Ameer-Beg, M. K. Y. Hughes, M. D. Keppler, S. Prag, M. Marsh, B. Vojnovic, and T. Ng. 2005. Multiphoton-FLIM quantification of the EGFP-mRFP1 RRET pair for localization of membrane receptor-kinase interactions. *Biophys. J.* 88:1224–1237.

43. Tzahar, E., H. Waterman, X. Chen, G. Levkowitz, D. Karunagaran, S. Lavi, B. J. Ratzkin, and Y. Yarden. 1996. A hierarchical network of interreceptor interactions determines signal transduction by Neu differentiation factor/neuregulin and epidermal growth factor. *Mol. Cell. Biol.* 16:5276–5287.

44. Zurita, A. R., P. M. Crespo, N. P. Koritschoner, and J. L. Daniotti. 2004. Membrane distribution of epidermal growth factor receptors in cells expressing different angliosides. *Eur. J. Biochem.* 271:2428–2437.

45. Xia, Z., and Y. Liu. 2001. Reliable and global measurement of fluorescence resonance energy transfer using fluorescence microscopes. *Biophys. J.* 81:2395–2402.

46. Dinger, M. C., J. E. Bader, A. D. Kóbor, A. K. Kretzschmar, and A. G. Beck-Sickinger. 2003. Homodimerization of neuropeptide Y receptors investigated by fluorescence resonance energy transfer in living cells. *J. Biol. Chem.* 278:10562–10571.

47. Grailhe, R., F. Merola, J. Ridard, S. Couvignou, C. Le Poupon, J.-P. Changeux, and H. L.-Pasquier. 2006. Monitoring protein interactions in the living cell through the fluorescence decays of the cyan fluorescent protein. *ChemPhysChem.* 7:1442–1454.

48. Zhang, X., J. Gureasko, K. Shen, P. A. Cole, and J. Kuriyan. 2006. An allosteric mechanism for activation of the kinase domain of epidermal growth factor receptor. *Cell.* 125:1137–1149.

49. Garrett, T. P. J., N. M. McKern, M. Lou, T. C. Elleman, T. E. Adams, G. O. Lovrecz, H.-J. Zhu, F. Walker, M. J. Frenkel, P. A. Hoyne, R. N. Jorissen, E. C. Nice, et al. 2002. Crystal structure of a truncated epidermal growth factor receptor extracellular domain bound to transforming growth factor $\alpha$. *Cell.* 110:763–773.

50. Ogiso, H., R. Ishitani, O. Nureki, S. Fukai, M. Yamanaka, J.-H. Kim, K. Saito, A. Sakamoto, M. Inoue, M. Shirouzu, and S. Yokoyama. 2002. Crystal structure of the complex of human epidermal growth factor and receptor extracellular domains. *Cell.* 110:775–787.

51. Ferguson, K. M., M. B. Berger, J. M. Mendrola, H.-S. Cho, D. J. Leahy, and M. A. Lemmon. 2003. EGF activates its receptor by removing interactions that autoinhibit ectodomain dimerization. *Mol. Cell.* 11:507–517.

52. Cho, H.-S., K. Mason, K. X. Ramyar, A. M. Stanley, S. B. Gabelli, D. W. Denney Jr., and D. J. Leahy. 2003. Structure of the extracellular region of HER2 alone and in complex with the Herceptin Fab. *Nature*. 421:756–760.

53. Garrett, T. P. J., N. M. McKern, M. Lou, T. C. Elleman, T. E. Adams, G. O. Lovrecz, M. Kofler, R. N. Jorissen, E. C. Nice, A. W. Burgess, and C. W. Ward. 2003. The crystal structure of a truncated ErbB2 ectodomain reveals an active conformation, poised to interact with other ErbB receptors. *Mol. Cell.* 11:495–505.

54. Walker, F., S. G. Orchard, R. N. Jorissen, N. E. Hall, H.-H. Zhang, P. A. Hoyne, T. E. Adams, T. G. Johns, C. Ward, T. P. J. Garrett, H.-J. Zhu, M. Nerrie, et al. 2004. CR1/CR2 interactions modulate the functions of the cell surface epidermal growth factor receptor. *J. Biol. Chem.* 279:22387–22398.

55. Wilkinson, J. C., and J. V. Staros. 2002. Effect of ErbB2 coexpression on the kinetic interactions of epidermal growth factor with its receptor in intact cells. *Biochemistry.* 41:8–14.

56. Saffarian S., Y. Li, E. L. Elson, and L. J. Pike. 2007. Oligomerization of the EGF receptor investigated by live cell fluorescence intensity distribution analysis. *Biophys. J.* (Epub ahead of print.)

57. Stamos, J., M. X. Slikowski, and C. Eigenbrot. 2002. Structure of the epidermal growth factor receptor kinase domain alone and in complex with a 4-anilinoquinazoline inhibitor. *J. Biol. Chem.* 277:46265–46272.

58. Mendrola, J. M., M. B. Berger, M. C. King, and M. A. Lemmon. 2002. The single transmembrane domains of ErbB receptors self-associate in cell membranes. *J. Biol. Chem.* 277:4704–4712.